

A full calculation of Zr and Sn isotopes in the Relativistic Mean Field theory

L.S. Geng^{a,c}, H. Toki^{a,b}, and J. Meng^c

^a*Research Center for Nuclear Physics (RCNP), Osaka University,
Ibaraki, Osaka 567-0047, Japan*

^b*The Institute of Physical and Chemical Research (RIKEN),
Wako, Saitama 351-0198, Japan*

^c*School of Physics, Peking University, Beijing 100871, P.R. China*

Abstract

The ground-state properties of Zr and Sn isotopes are studied within the relativistic mean field theory. Zr and Sn isotopes have received tremendous attentions due to various reasons, including the predicted giant halos in neutron-rich Zr isotopes, the unique feature of being robust spherical in the region of $^{100}\text{Sn} \sim ^{132}\text{Sn}$ and the particular interest of Sn isotopes to nuclear astrophysics. Furthermore, four magic numbers, 40, 50, 82 and 126, make these two isotopes particularly important to test a microscopic model. In the present work, we carry out a full calculation of Zr and Sn isotopes from the proton drip line to the neutron drip line with deformation, pairing correlations and blocking effect for even-odd nuclei included. A quadrupole constrained calculation is performed to find the absolute minimum for each nucleus. All ground-state properties, including separation energies, odd-even staggering (OES), nuclear radii, deformations and single-particle spectra are analyzed and discussed in detail.

1 Introduction

One of the main aims of researches in nuclear physics is to try to describe ground-state properties of nuclei in the whole mass region. Unfortunately, due to lack of understanding in strong interaction and numerical difficulty in treating nuclear many-body problems, so far all microscopic descriptions are only possible on a phenomenological ground. The most successful theories of this type are conventional Hartree-Fock model with effective density-dependent interactions [1,2] and its relativistic analog, the relativistic mean field (RMF) theory [3,4,5]. Compared with Hartree-Fock method, RMF theories begin on a more microscopic level, since they treat both nucleonic and mesonic degrees

of freedom and are fully relativistic. Therefore, spin is included automatically without any additional parameters, which leads naturally to proper spin-orbit interaction. Such a property is believed to be very important for studying nuclei with extreme isospin values, which have become accessible in recent years due to developments in accelerator technology and detection techniques [6]. The RMF method has been very successful for the description of many nuclear properties including binding energies, nuclear radii and deformations [5,7] from the proton drip line to the neutron drip line. However, the number of properties investigated by the RMF method is still considerably less than those done by its non-relativistic counterpart.

To describe nuclear ground-state properties reliably, one must take into account both deformation effects and pairing correlations simultaneously. An extensive study of even-even nuclei over the entire mass region by Hirata et al. [8] shows that most nuclei are deformed except for a few with magic numbers. In the present work, the deformation is treated by using the expansion method in the axially-symmetric Harmonic-Oscillator basis first introduced into the RMF method by Gambhir et al. [9]. In their original work, the pairing correlation is treated by a constant pairing interaction with a pairing window, which has been found to be incapable of describing drip-line nuclei. On the other hand, a delta-function interaction in the particle-particle channel has been found to be able to take into account the couplings to the continuum properly by different authors both in relativistic [10,11,12,13] and non-relativistic [14] mean field models. We, therefore, introduced the delta-function interaction into the axially-symmetric treatment of the RMF method and demonstrated its applicability in Ref. [15]. We have applied this method to study properties of light nuclei [16], particularly proton skin in Ar isotopes and neutron skin in Na isotopes, ground-state properties of deformed proton emitters [17] and alpha-decay properties of lately synthesized superheavy elements [18] with $Z=115$ and 113 . All these works show that this method is both effective and efficient. Also we conclude that a reliable calculation should include deformation, proper pairing correlations and blocking treatment of nuclei with odd-number nucleons. When applying this method to neutron-rich nuclei, due to their large spacial extension, we can not expect that it reproduce fully the sudden increase of neutron radii for halo nuclei, which is found if we have solved the RMF equations in coordinate space [13,15,19]. However, except for neutron radii of halo nuclei, other properties can be reproduced with satisfactory accuracy by this method [15]. The other possibilities is to use a Woods-Saxon basis obtained by solving either the Schrödinger equation or the Dirac equation the solution with a Woods-Saxon potential[20].

Zr and Sn isotopes are two very interesting isotopes in the periodic table. Zr has a semi-magic proton number, $Z = 40$, and its neutron number can be magic-numbers 40, 50 and 82. Several previous RMF calculations show that the so-called giant halos may occur in Zr isotopes when neutron number goes

beyond 82 [13,15,19]. While Sn isotopes has long been of special interest for nuclear physicists not only because it has a magic proton number, $Z = 50$, but also due to its long isotopic chain. Experimentally both neutron deficient ^{100}Sn and neutron-rich ^{134}Sn have been produced. We expect that its isotopes will even extend to next neutron magic number, $N = 126$, which will be seen in the present work. Both experimentally and theoretically most Sn isotopes have been found to be spherical, particularly those nuclei with $N = 50 \sim 82$, but whether or not such a trend can continue to the next neutron-magic number, $N = 126$, remains to be an interesting question. Recently, Samanta et al. suggested that $Z = 82$ loses its magicity around $N = 106$ based on the extended Bethe-Weizsäcker mass formula [21]. This motivates us to study also the magicity of $Z = 50$ by the RMF method. Just like Zr isotopes, Sn isotopes have also been investigated quite a lot both in relativistic [22,23,24] and non-relativistic mean field theory [25]. However, most of them are limited to either spherical assumptions or even-even nuclei or just part of the whole isotopic chain. The same limitations are also true for Zr isotopes. For Zr isotopes, to confirm the interesting conclusion of spherical case that giant halos may occur in this isotopic chain and study the behaviors of even-odd nuclei in the neutron-drip line region, a detailed calculation including deformation, proper pairing correlations and blocking treatment is necessary. Such a calculation is also needed for Sn isotopes in order to study neutron-rich nuclei with as many effects as possible being considered.

In the present work, we apply the recently formulated deformed RMF+BCS method with a density-independent delta-function interaction in the pairing channel [15,16,17,18] to the analysis of ground-state properties of Zr and Sn isotopes from the proton drip line to the neutron drip line. In particular, we want to study the drip-line nuclei in both isotopes, odd-even staggering (OES) through the isotopic chains and the magicity of $Z = 50$ in the neutron-rich region. We use the TMA parameter set for our RMF Lagrangian density, which has been proved to be very successful in various regions. In Sect. 2, we shall present the RMF theory with deformation and pairing correlations. The numerical results will be presented in Sect. 3 for Zr and Sn isotopes and a summary of the present study is given in Sect. 4.

2 Relativistic mean field theory with deformation and pairing correlations

We present here the formulation of the RMF theory with deformation and pairing correlations. We employ the model Lagrangian density with nonlinear terms for both σ and ω mesons, as described in detail in Ref. [26], which is

given by

$$\begin{aligned}
\mathcal{L} = & \bar{\psi}(i\gamma^\mu\partial_\mu - M)\psi + \frac{1}{2}\partial_\mu\sigma\partial^\mu\sigma - \frac{1}{2}m_\sigma^2\sigma^2 - \frac{1}{3}g_2\sigma^3 - \frac{1}{4}g_3\sigma^4 - g_\sigma\bar{\psi}\sigma\psi \\
& - \frac{1}{4}\Omega_{\mu\nu}\Omega^{\mu\nu} + \frac{1}{2}m_\omega^2\omega_\mu\omega^\mu + \frac{1}{4}g_4(\omega_\mu\omega^\mu)^2 - g_\omega\bar{\psi}\gamma^\mu\psi\omega_\mu \\
& - \frac{1}{4}R^a{}_{\mu\nu}R^{a\mu\nu} + \frac{1}{2}m_\rho^2\rho_\mu^a\rho^{a\mu} - g_\rho\bar{\psi}\gamma_\mu\tau^a\psi\rho^{\mu a} \\
& - \frac{1}{4}F_{\mu\nu}F^{\mu\nu} - e\bar{\psi}\gamma_\mu\frac{1-\tau_3}{2}A^\mu\psi,
\end{aligned} \tag{1}$$

where the field tensors of the vector mesons and of the electromagnetic field take the following forms:

$$\begin{cases} \Omega_{\mu\nu} = \partial_\mu\omega_\nu - \partial_\nu\omega_\mu \\ R^a{}_{\mu\nu} = \partial_\mu\rho_\nu^a - \partial_\nu\rho_\mu^a - 2g_\rho\epsilon^{abc}\rho_\mu^b\rho_\nu^c \\ F_{\mu\nu} = \partial_\mu A_\nu - \partial_\nu A_\mu \end{cases} \tag{2}$$

and other symbols have their usual meanings. Based on the single-particle spectrum calculated by the RMF method described above, we perform a state-dependent BCS calculation [27,28]. The gap equation has a standard form for all the single particle states. i.e.

$$\Delta_k = -\frac{1}{2} \sum_{k'>0} \frac{\bar{V}_{kk'}\Delta_{k'}}{\sqrt{(\varepsilon_{k'} - \lambda)^2 + \Delta_{k'}^2}}, \tag{3}$$

where $\varepsilon_{k'}$ is the single particle energy and λ is the Fermi energy. The particle number condition is given by $2 \sum_{k>0} v_k^2 = N$. In the present work we use a delta-force for the pairing interaction, i.e.

$$V = -V_0\delta(\mathbf{r}_1 - \mathbf{r}_2), \tag{4}$$

with the same strength V_0 for both protons and neutrons. The pairing matrix element for the delta-function interaction is given by

$$\bar{V}_{ij} = \langle i\bar{i}|V|j\bar{j}\rangle - \langle i\bar{i}|V|\bar{j}j\rangle = -V_0 \int d^3r \left[\psi_i^\dagger\psi_i^\dagger\psi_j\psi_{\bar{j}} - \psi_i^\dagger\psi_i^\dagger\psi_{\bar{j}}\psi_j \right] \tag{5}$$

with nucleon wave function in the form

$$\psi_i(\mathbf{r}, t) = \begin{pmatrix} f_i(\mathbf{r}) \\ ig_i(\mathbf{r}) \end{pmatrix} = \frac{1}{\sqrt{2\pi}} \begin{pmatrix} f_i^+(z, r_\perp) e^{i(\Omega_i-1/2)\varphi} \\ f_i^-(z, r_\perp) e^{i(\Omega_i+1/2)\varphi} \\ ig_i^+(z, r_\perp) e^{i(\Omega_i-1/2)\varphi} \\ ig_i^-(z, r_\perp) e^{i(\Omega_i+1/2)\varphi} \end{pmatrix} \chi_{t_i}(t). \quad (6)$$

A detailed description of the deformed RMF+BCS method can be found in Ref. [9,15].

In the present study, nuclei with both even and odd number of protons (neutrons) need to be calculated. We adopt a simple blocking method without breaking the time reversal symmetry. The ground state of an odd system is described by the wave function,

$$\alpha_{k_1}^\dagger |BCS\rangle = \alpha_{k_1}^\dagger \prod_{k \neq k_1} (u_k + v_k \alpha_k^\dagger \alpha_k^\dagger) |vac\rangle. \quad (7)$$

Here, $|vac\rangle$ denotes the vacuum state. The unpaired particle sits in the level k_1 and blocks this level. The Pauli principle prevents this level from participating in the scattering process of nucleons caused by the pairing correlations. As described in Ref. [28], in the calculation of the gap, one level is "blocked":

$$\Delta_k = -\frac{1}{2} \sum_{k' \neq k_1 > 0} \frac{\bar{V}_{kk'} \Delta_{k'}}{\sqrt{(\varepsilon_{k'} - \lambda)^2 + \Delta_{k'}^2}}. \quad (8)$$

The level k_1 has to be excluded from the sum, because it can not contribute to the pairing energy. The corresponding chemical potential is determined by

$$N = 1 + 2 \sum_{k \neq k_1 > 0} v_k^2. \quad (9)$$

The blocking procedure is performed at each step of the self-consistent iteration.

3 Numerical results and discussions

In the present work we use the mass-dependent parameter set TMA [26,29] for the RMF Lagrangian. The calculations for the present analysis have been carried out by an expansion in 20 oscillator shells for both fermion fields and

boson fields, which are found to be enough for the present purpose. Following Ref. [9], we fix $\hbar\omega_0 = 41A^{-1/3}$ for fermions. In the pairing channel, pairing strength $V_0 = 341.1 \text{ Mev fm}^3$ is used for Zr isotopes and $V_0 = 310.0 \text{ Mev fm}^3$ is used for Sn isotopes, which are obtained by fitting the experimental odd-even staggering (OES) of Zr and Sn isotopes. Using the same pairing strength for Sn isotopes as the one for Zr isotopes will end with generally overestimated odd-even staggering (OES). For each nucleus, first the quadrupole constrained calculation [30] is done to obtain all possible ground-state configurations; second we perform the non-constrained calculation using the quadrupole deformation parameter of the deepest minimum of the energy curve of each nucleus as the deformation parameter for our Harmonic-Oscillator basis. In the case of several similar minima from the constrained calculation, we repeat the above procedure to obtain the configuration with the lowest energy as our final result. We stress that such a procedure can find the absolute minimum for both even-even and even-odd nuclei. In what follows we discuss the details of our calculations and the numerical results. To save space, we don't include a detailed tabulation of all the ground-state properties we obtained. All the data are available on our home page (<http://rcnp.osaka-u.ac.jp/~lsgeng0>) and also available upon request.

Double and single neutron separation energies

$$S_{2n}(Z, N) = B(Z, N) - B(Z, N - 2), \quad (10)$$

$$S_n(Z, N) = B(Z, N) - B(Z, N - 1), \quad (11)$$

are displayed in Figs. 1 and 2 for Zr isotopes and Sn isotopes, respectively, from the proton drip line to the neutron drip line. Results obtained from the deformed RMF+BCS calculations with the parameter set TMA are compared with available experimental data [31]. It is clearly seen that both experimental separation energies and OES are reproduced quite well by the theoretical calculations.

For Zr isotopes, despite of the fact that they are largely deformed for some Zr nuclei (see Figs. 4 ~ 6), the agreement between theory and experiment is very good. The experimental feature that the OES is larger for nuclei with $N = 40 \sim 50$ than for nuclei with $N = 51 \sim 68$ is also reproduced quite well. Both double and single neutron separation energies are quite small for nuclei with $N > 82$. The so-called giant halos are predicted to exist in this region by both RCHB [19] and resonant RMF+BCS [13] calculations with spherical assumptions. Our previous deformed RMF+BCS calculations [15] reached the same conclusion and confirmed that the expansion method in Harmonic-Oscillator basis can provide very accurate results for nuclear binding energies even in the neutron-rich region. All these calculations [13,15,19], however, studied only even-even nuclei. From the lower panel of Fig. 1, we notice that the

OES of Zr isotopes with $N > 82$ are quite small and S_n of those nuclei with odd mass numbers are almost zero or negative. This confirmed the belief that pairing interaction can increase binding energies of even-even nuclei and therefore contribute the formation of halo nuclei. We also conclude that generally we will see one-neutron halo nuclei first and then only two-neutron halo nuclei are stable due to pairing interaction. The same conclusion also holds for Sn isotopes.

For Sn isotopes, we notice that the agreement between theory and experiment is very good in the region, $^{115}\text{Sn} \sim ^{132}\text{Sn}$. For nuclei with $N \leq 64$, the theoretical OES drops a little bit suddenly. The reason behind this is a relatively large spin-orbit splitting between $2d_{5/2}$ state and $2d_{3/2}$ state, around 1.8 MeV in our present calculations (see Fig. 9), which makes pairing energy in nuclei with $N \leq 64$ smaller than nuclei with $N = 64 \sim 82$. We note that the smaller OES in the region of $^{146}\text{Sn} \sim ^{160}\text{Sn}$ is complicated and maybe related with two different phenomena. One is that nuclei in this region are deformed (see Figs. 4 and 6). The other is that as we shall see from Fig. 9, $3p_{1/2}$, $2f_{5/2}$ and $3p_{3/2}$ states, which become occupied in this region, are quite close to each other in the spherical case. We believe that this feature is important for Sn isotopes to stay stable till ^{176}Sn . In both isotopes, we should note that for nuclei with $N \approx Z$ additional residual interactions, such as proton-neutron pairing, will contribute and increase the OES somewhat, which are not included in our method. Unlike Zr isotopes, we don't see a clear indication of possible two-neutron halo in Sn isotopes, which is consistent with all previous calculations. The double neutron separation energy goes directly to about -2.5 MeV for ^{178}Sn from about 1.4 MeV for ^{176}Sn . However, from the lower panel of Fig.2, we can see that S_n stays below 1.0 MeV from ^{157}Sn till the end of this isotopic chain, which probably implies possible existence of one-neutron halo.

The larger predicted gaps than experiment for $N = 50$ in Zr isotopes and $N = 82$ in Sn isotopes seem to indicate that the parameter TMA overestimates these major gaps a little bit. We find that this feature is common to almost all existing parameter sets [32]. This suggests that the usual parameter fitting method, which fits binding energies and charge radii of a few selected spherical nuclei, should be improved to take into account the single-particle spectra from the very beginning.

The average binding energies of Zr and Sn isotopes are plotted as functions of mass number A in Fig. 3. It can be clearly seen that the theoretical predictions reproduce the experimental data accurately including the OES in Sn isotopes. For Zr isotopes, the small deviation between theory and experiment for nuclei with $N = 90 \sim 98$ may relate to the possible γ -deformation, which are not included here. We hope that this deviation can be reduced if we use a particle-number conserved version of BCS method. This work is in progress now. For Sn isotopes around $N \approx Z$, our calculated results are somewhat larger than

experimental values.

Deformation is an quite important property for nuclei, because it can increase nuclear binding energy so that a deformed shape is more favored than spherical shape for some nuclei. It has been argued that in light- or medium-mass nuclei deformation provides the same amount of OES as the pairing interaction [33] and/or that the OES in light nuclei is a mere reflection of the deformed mean field [34]. Although it is believed that the OES in heavy nuclei is mainly due to pairing correlations, the deformation effect should not be ignored. We have shown also in Ref. [15] that deformation in even-even Zr isotopes is quite important to reduce the discrepancy between theoretical and experimental binding energies. $Z = 50$ have long been thought as a special magic number in the sense that all Sn isotopes are believed to be spherical. Whether or not Sn isotopes are deformed also is of special interest to the production of nuclei both in the laboratory and in astrophysical process.

In Fig. 4, we plot the mass quadrupole deformation parameters, β_2 , for Zr and Sn isotopes. Our method have been shown to be able to describe nuclear deformation quite well in a wide mass region [15,16,17]. First, we see for Zr isotopes that the deformation is quite complicated. It starts from the neutron-deficient side as being strongly prolate ($\beta_2 \sim 0.6$), then goes oblate-prolate-oblate-prolate and ends as being oblate ($\beta_2 \sim -0.2$). However, Sn isotopes are quite different. It remains spherical till N reaches 88. Then, we see a similar feature as that appears at the neutron-rich side of Zr isotopes. Nuclei with $N > 108$ becomes spherical again till the end of the Tin isotopic chain. It is a quite interesting feature first observed in RMF calculations. Since these neutron-rich isotopes are still far beyond the reach of present experimental ability, we hope that this finding can be checked by future works both theoretically and experimentally. Another interesting thing we notice is that the even-odd nucleus tends to be deformed despite that its neighboring even-even nuclei are all spherical. Of course at most of times, the deformation is quite small and we can say that it is essentially spherical. Most even-odd Sn isotopes belong to this group. However, in Zr isotopes, some even-odd nuclei differer from their even-even neighbors by an absolute β_2 of 0.1. ^{87}Zr , ^{89}Zr , ^{117}Zr and ^{119}Zr are such examples.

Usually, we can find two minima, one prolate and one oblate, or one spherical minimum in axially-deformed nuclei. On the theoretical side, it is easy to tell which one is the ground-state configuration if the difference between total energies of different minima is relatively large. On the other hand, nuclei in transition region often have two minima with similar total energies, where it is difficult to determine the ground state without ambiguity. ^{82}Zr , ^{86}Zr , ^{93}Zr and ^{116}Zr are such examples in Zr isotopes. We display their total energy curves together with those of 12 other Zr isotopes as functions of β_2 in Fig. 5. It provides us a vivid picture how deformation evolves in Zr isotopes. Nuclei with

$A < 82$ are strongly prolate with $\beta_2 \approx 0.5$. At ^{82}Zr , the oblate configuration becomes as stable as the prolate configuration. Nuclei with $82 < A < 86$ are moderately oblate with $\beta_2 \approx -0.2$. At ^{86}Zr , the total energy curve becomes quite flat at the bottom and the spherical configuration is a little bit more stable. With increasing N , even-even nuclei stay almost spherical while even-odd nuclei are somewhat deformed. At ^{93}Zr , the prolate configuration $\beta_2 \approx 0.2$ is more stable than the oblate configuration $\beta_2 \approx -0.1$. Nuclei with increasing N become more prolate and reaches $\beta_2 \approx 0.4$ at ^{109}Zr . Then it becomes oblate in ^{110}Zr and begins to become spherical with increasing N . At ^{116}Zr , it reaches the spherical configuration and stays spherical for even-even nuclei till ^{124}Zr . Then it becomes more and more prolate till ^{129}Zr and from ^{130}Zr it stays moderately oblate, $\beta_2 \approx -0.2$, till the end of this isotopic chain. It will be very interesting to study shape-coexistence in Zr isotopes and compare with experimental data, if available.

Different ground-state deformations are found for proton and neutron density distributions in exotic nuclei. In Fig. 6, proton deformation parameters β_{2p} are compared with neutron deformation parameters β_{2n} for Zr and Sn isotopes, respectively. It shows that these two quantities are almost the same for most nuclei. For both neutron drip-line nuclei in Zr and Sn isotopes, $|\beta_{2n}|$ is larger than $|\beta_{2p}|$ in the deformed region, which means that the deformation driving force is from the neutron side. While in the spherical region, there are no visible differences between β_{2p} and β_{2n} .

From proton (neutron) density distributions, $\rho_{p(n)}$, we can easily deduce the corresponding proton (neutron) radius,

$$R_{p(n)} = \langle r_{p(n)}^2 \rangle^{1/2} = \left[\frac{\int \rho_{p(n)} r^2 d\mathbf{r}}{\int \rho_{p(n)} d\mathbf{r}} \right]^{1/2}. \quad (12)$$

The charge radius, R_c , is related to the proton radius, R_p , after considering the finite size of the proton, by

$$R_c^2 = R_p^2 + 0.64 \quad [\text{fm}]. \quad (13)$$

We display in Figs. 7 and 8 the charge, proton and neutron rms radii for Zr and Sn isotopes. The calculated charge radii are compared with experimental data from Ref. [35]. Excellent agreement between theory and experiment can be clearly seen. We can also see the effect of deformation easily from Figs. 7 and 8, and that Zr isotopes are more complicated than Sn isotopes. In the upper panel of Fig. 7, R_c of Zr isotopes drops dramatically for ^{82}Zr and ^{110}Zr , which is due to deformation effect. If we look at Fig. 6, it becomes much clearer: β_{2p} changes from 0.535 for ^{81}Zr to -0.218 for ^{82}Zr ; correspondingly, β_{2n} changes from 0.418 for ^{109}Zr to -0.216 for ^{110}Zr . There are also some abnormalities in

Sn isotopes as we can see clearly in the upper panel of Fig. 8, which have the same origins as Zr isotopes. β_{2p} jumps from 0.085 for ^{144}Sn to 0.220 for ^{145}Sn and it changes from -0.244 for ^{157}Sn to 0.0 for ^{158}Sn .

In the lower panels of Figs. 7 and 8, we plot R_n and R_p together in order to see the differences between them easily. We also display a solid line with a $N^{1/3}$ dependence in both panels for R_n . It is quite clear that neutron-rich nuclei in Zr isotopes deviate from the $N^{1/3}$ line quite a lot, which implies that the giant halos exist even though deformation develops after $N = 82$. While for Sn isotopes our calculated results agree well with the $N^{1/3}$ line. The difference between R_n and R_p , i.e. neutron skin, reaches 0.9 fm for ^{140}Zr and 0.8 fm for ^{176}Sn , which can be viewed as another indication of possible existing neutron halo in Zr isotopes. Of course, we should note that as we have found in our previous work [15], the sudden increase of neutron radii in $^{124}\text{Zr} \sim ^{140}\text{Zr}$, predicted by RCHB [19] and resonant RMF+BCS [13] calculations, can not be fully reproduced by our expansion method in Harmonic-Oscillator basis. Nevertheless, this should not prevent us from gaining some useful insights into possible neutron halo feature, as we can see in Zr isotopes where a sudden increase in neutron radii from ^{123}Zr is quite obvious.

In our above discussions, the discrepancies in the single-neutron separation energies for Sn isotopes with $N < 64$ have been attributed to single-particle spectra. The abnormalities in the region of $^{146}\text{Sn} \sim ^{160}\text{Sn}$ are also related to the corresponding shell structure. To see all these more clearly, we display the neutron single-particle spectra of five nuclei in Sn isotopes, i.e. ^{100}Sn , ^{114}Sn , ^{132}Sn , ^{158}Sn and ^{176}Sn in Fig. 9. These isotopes are so chosen to represent the whole Sn isotopes from the proton drip line to the neutron drip line and also include two typical nuclei in the region where the predicted OES changes abruptly. All the five nuclei are spherical in our calculations. It is quite clear that $1h_{11/2}$, $3s_{1/2}$ and $2d_{3/2}$ states are quite close to each other, which explains the somewhat large difference in the OES between nuclei with $N > 64$ and $N < 64$, together with the relatively larger gap between $2d_{3/2}$ state and $2d_{5/2}$ state. The small gap between $3p_{1/2}$, $2f_{5/2}$ and $3p_{3/2}$ states is possibly responsible for both the deformation phenomena and abnormalities in the OES in the region of $^{146}\text{Sn} \sim ^{160}\text{Sn}$.

There are some other important features shown in Fig. 8. First, the neutron level density increases with N . For example, the single-particle energy of $1s_{1/2}$ state increases about 10.0 MeV from about -62.0 MeV in ^{100}Sn to -52.0 MeV in ^{176}Sn . Meanwhile, the single-particle energy of $1g_{9/2}$ state decreases about 2.0 MeV. Second, it is quite clear that spin-orbit splitting decreases with increasing N . Some obvious spin-orbit partners are $(1p_{1/2}, 1p_{3/2})$, $(1d_{3/2}, 1d_{5/2})$, $(1f_{5/2}, 1f_{7/2})$ and $(1g_{7/2}, 1g_{9/2})$. The decrease of spin-orbit splitting with increasing N in the relativistic mean field theory has been discussed in several previous works (see Ref. [23]), where it has been attributed to the diffuseness

of the potential or the outward push of the potential.

4 Conclusions

The relativistic mean field theory has been very successful in the description of many nuclear ground-state properties. It also predicts a lot of very interesting phenomena for nuclei with extreme isospin values. The two-neutron halo in ^{11}Li was successfully explained by this method[10]. It also predicts possible two-neutron halos in several regions of the periodic table, such as Ca and Zr isotopes[13,15,19,36]. It is our strong desire to develop a model valid for all nuclei, including unstable ones from the proton drip line to the neutron drip line. The relativistic mean field theory, as a relativistic method which incorporates spin-orbit interaction naturally, hopefully can be the desirable model with only a few parameters fitted by ground-state properties of a few selected spherical nuclei. However, to describe all nuclei in the periodic table, deformation and pairing correlations must be included properly. The present method we adopted can fulfill all these requirements and cost reasonable time to carry out large-scale calculations covering all nuclei over the entire mass region, which are absolutely necessary to test a phenomenological method.

In the present work, we study two interesting isotopes, Zr and Sn isotopes, which are very important in both nuclear physics and nuclear astrophysics, and have received tremendous attentions. Our calculations reproduce available experimental data very well including binding energies, OES and charge radii. We confirmed the previous calculations that two-neutron halo can occur in Zr isotopes. We also find that one-neutron halo is possible for this isotopic chain, which will appear simultaneously with two-neutron halo and disappear earlier than two-neutron halo. No obvious two-neutron halo is found in Sn isotopes in the aspects of both two-neutron separation energies and neutron radii. However, one-neutron halo is possible based on one-neutron separation energies. Surprisingly, we find that Sn isotopes go till the neutron magic number 126 and are deformed in the region of $N = 89 \sim 107$, which could be viewed as loss of magicity of $Z = 50$ around this region. Some even-odd nuclei are found to be deformed despite that their even-even neighbors are spherical in both these two isotopic chains. The somewhat large gaps for $N = 50$ in Zr isotopes and $N = 82$ in Sn isotopes seem to suggest that the usual parameter fitting method should be improved in order to take into account single-particle spectra from the very beginning.

5 Acknowledgments

L.S. Geng is grateful to the Monkasho fellowship for supporting his stay at Research Center for Nuclear Physics where this work is done. This work was partly supported by the Major State Basic Research Development Program Under Contract Number G2000077407 and the National Natural Science Foundation of China under Grant No. 10025522, 10221003 and 10047001.

References

- [1] J. Decharge and D. Gogny, *Phys. Rev. C* 21 (1980) 1568.
- [2] H. Flocard, P. Quentin and D. Vautherin, *Phys. Lett. B* 46 (1973) 304.
- [3] B.D. Serot and J.D. Walecka, *Adv. Nucl. Phys.* 16 (1986) 1.
- [4] P.G. Reinhard, *Rep. Prog. Phys.* 52 (1989) 439.
- [5] P. Ring, *Prog. Part. Nucl. Phys.* 37 (1996) 193.
- [6] I. Tanihata, *Prog. Part. Nucl. Phys.* 35 (1995) 505.
- [7] D. Hirata, H. Toki, T. Watabe, I. Tanihata, and B. V. Carlson, *Phys. Rev. C* 44 (1991) 1467.
- [8] D. Hirata, K. Sumiyoshi, I. Tanihata, Y. Sugahara and H. Toki, *Nucl. Phys. A* 616 (1997) 438c.
- [9] Y.K. Gambhir, P. Ring and A. Thimet, *Ann. Phys. (N.Y.)* 194 (1990) 132.
- [10] J. Meng and P. Ring, *Phys. Rev. Lett.* **77**, 3963 (1996).
- [11] J. Meng, *Nucl. Phys. A* 635 (1998) 3.
- [12] H.L. Yadav, S. Sugimoto and H. Toki, *Mod. Phys. Lett. A* 17 (2002) 2523.
- [13] N. Sandulescu, L.S. Geng, H. Toki and G. Hillhouse, *Phys. Rev. C* 68 (2003) 054323.
- [14] N. Sandulescu, Nguyen Van Giai and R.J. Liotta, *Phys. Rev. C* 61 (2000) R061301.
- [15] L.S. Geng, H. Toki, S. Sugimoto and J. Meng, *Prog. Theor. Phys.* 110 (2003) 921.
- [16] L.S. Geng, H. Toki, A. Ozawa and J. Meng, *Nucl. Phys. A* 730 (2004) 80.
- [17] L.S. Geng, H. Toki and J. Meng, *nucl-th/0309016*.
- [18] L.S. Geng, H. Toki and J. Meng, accepted by *Physics Review C*, in press.

- [19] J. Meng and P. Ring, Phys. Rev. Lett. 80 (1998) 460.
- [20] S. G. Zhou, J. Meng, P. Ring, Phys. Rev. C 68 (2003) 034323
- [21] C. Samanta et al., private communication; C. Samanta and S. Adhikari, Phys. Rev. C 65 (2002) 037301.
- [22] J. Meng, K.Sugawara-Tanabe, S.Yamaji, P. Ring and A.Arima, Phys. Rev. C58 (1998) R628. J. Meng, K. Sugawara-Tanabe, S. Yamaji and A. Arima, Phys. Rev. C 59 (1999) 154.
- [23] J. Meng, I. Tanihata, Nucl. Phys. A 650 (1999) 176.
- [24] G.A. Lalazissis, D. Vretenar and P. Ring, Phys. Rev. C 57 (1998) 2294.
- [25] Shouichi Sakakihara, Yasutoshi Tanaka, Nucl. Phys. A 691 (2001) 649.
- [26] Y. Sugahara and H. Toki, Nucl. Phys. A 579 (1994) 557.
- [27] A.M. Lane, *Nuclear Theory* (Benjamin, 1964).
- [28] P. Ring and P. Schuck, *The Nuclear Many-body Problem* (Springer, 1980).
- [29] Y. Sugahara, Doctor thesis in Tokyo Metropolitan University (1995).
- [30] H. Flocard et al., Nucl. Phys. A 203 (1973) 433.
- [31] G. Audi and A.H. Wapstra, Nucl. Phys. A 595 (1995) 409.
- [32] Wenhui Long, Jie Meng, Nguyen Van Giai, Shan-Gui Zhou, nucl-th/0311031.
- [33] W. Satula, J. Dobaczewski and W. Nazarewicz, Phys. Rev. Lett. 81 (1998) 3599.
- [34] H. Häkkinen et al., Phys. Rev. Lett. 78 (1997) 1034.
- [35] H. De Vries, C. W. De Jager and C. De Vries, At. Data Nucl. Data Tables 36 (1987) 495.
- [36] J. Meng, H. Toki, J. Y. Zeng, S. Q. Zhang and S.-G. Zhou, Phys. Rev. C 65(2002)041302(R) .

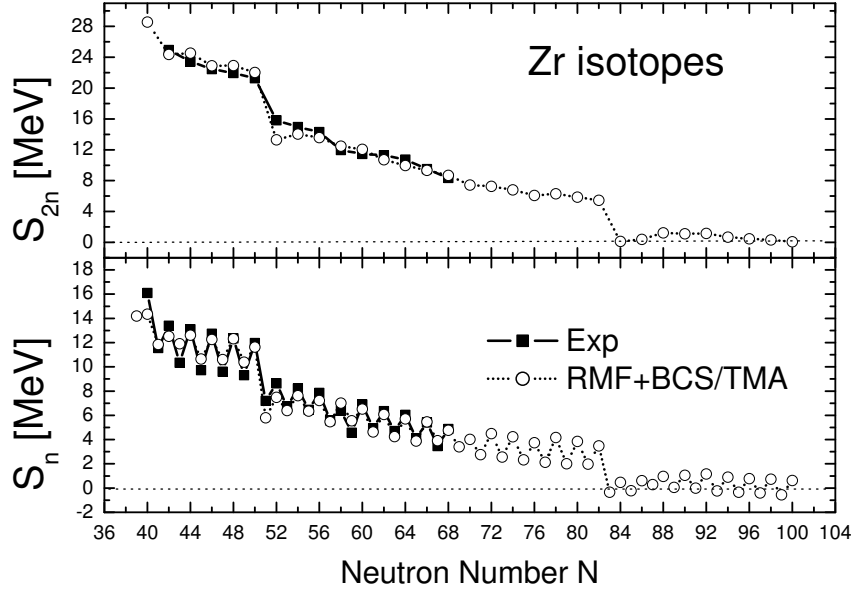


Fig. 1. The double and single neutron separation energies, S_{2n} and S_n , of Zr isotopes. Results obtained from the deformed RMF+BCS calculations with TMA set (open circle) are compared with available experimental data (solid square) [31].

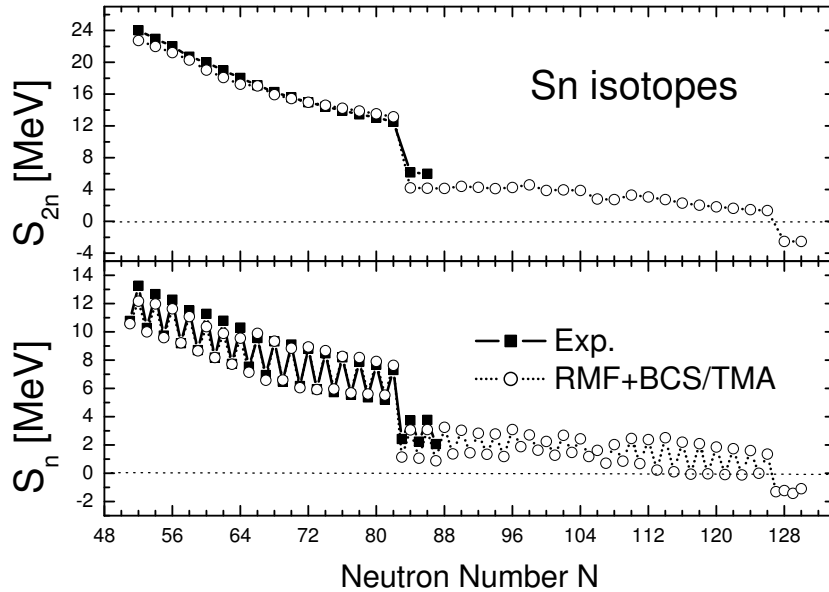


Fig. 2. The double and single neutron separation energies, S_{2n} and S_n , of Sn isotopes. Results obtained from the deformed RMF+BCS calculations with TMA set (open circle) are compared with available experimental data (solid square) [31].

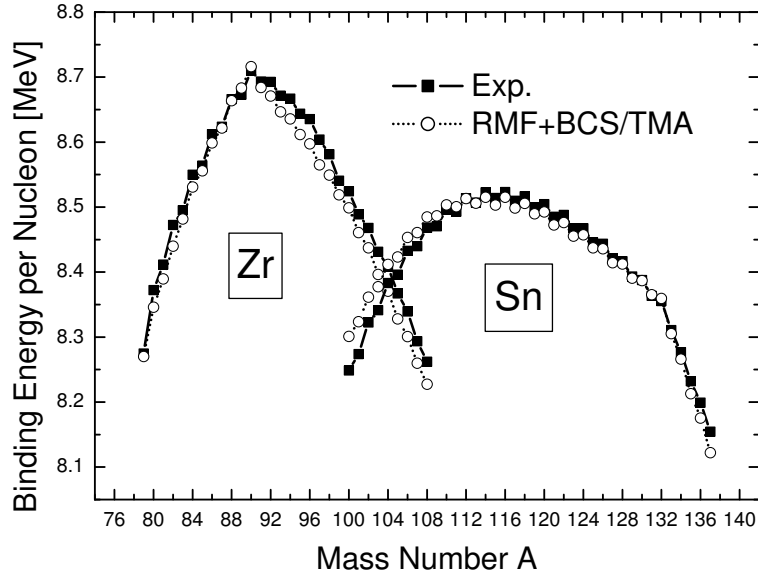


Fig. 3. The binding energies per nucleon of Zr and Sn isotopes. Results obtained from the deformed RMF+BCS calculations with TMA set (open circle) are compared with available experimental data (solid square) [31].

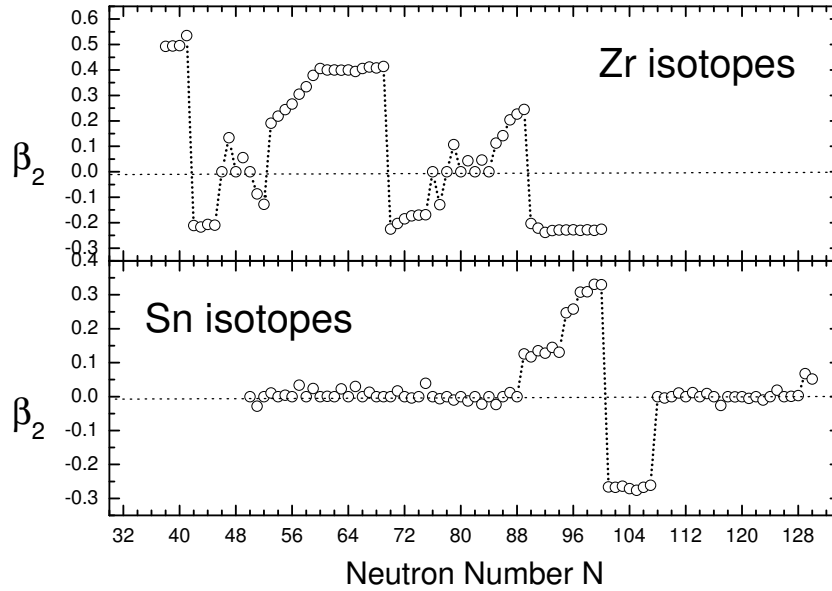


Fig. 4. Mass quadrupole deformation parameters, β_2 , of Zr and Sn isotopes obtained from the deformed RMF+BCS calculations with TMA set.

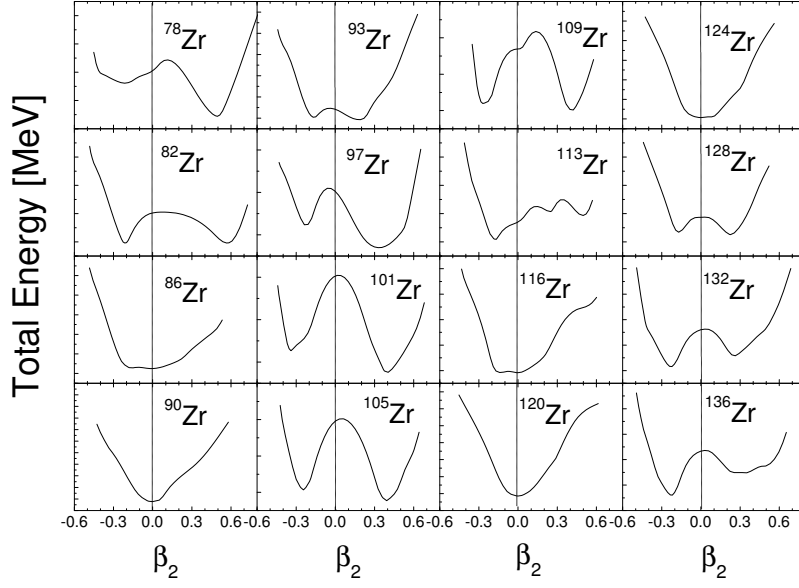


Fig. 5. Total energy curves of 16 Zr isotopes obtained from the deformed RMF+BCS calculations with TMA set as functions of mass quadrupole deformation parameters, β_2 .

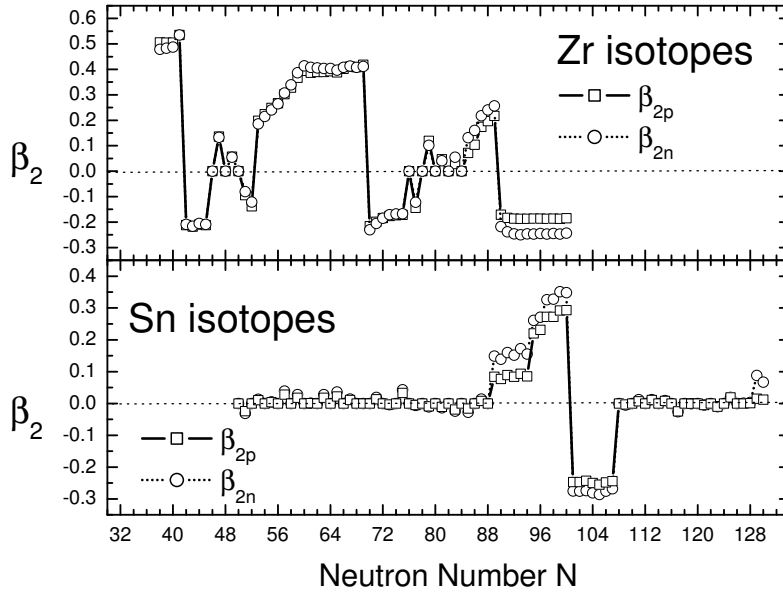


Fig. 6. Proton and neutron quadrupole deformation parameters, β_{2p} (open square) and β_{2n} (open circle), of Zr and Sn isotopes obtained from the deformed RMF+BCS calculations with TMA set.

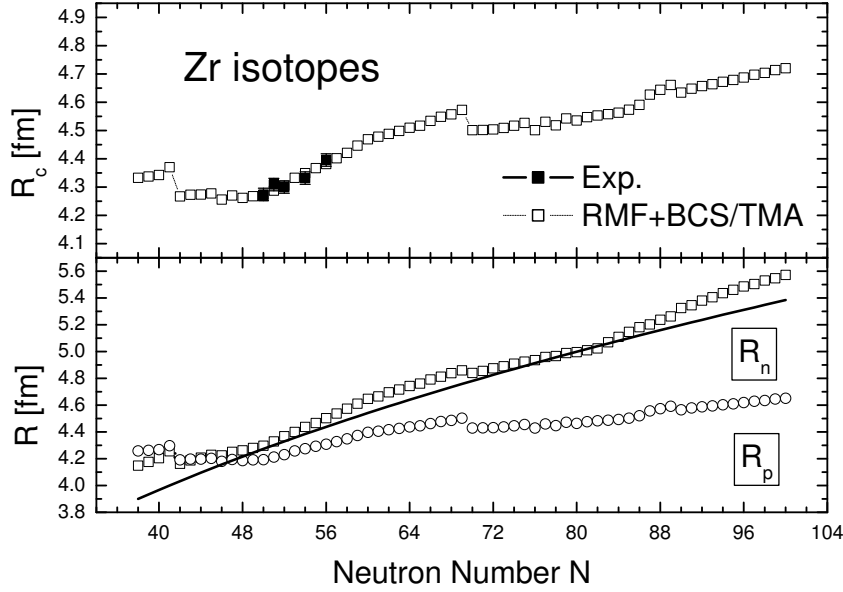


Fig. 7. Charge, proton and neutron radii obtained from the deformed RMF+BCS calculations with TMA set (open square and circle) compared with experimental data (solid square) [35]. The solid line denotes a $N^{1/3}$ dependence.

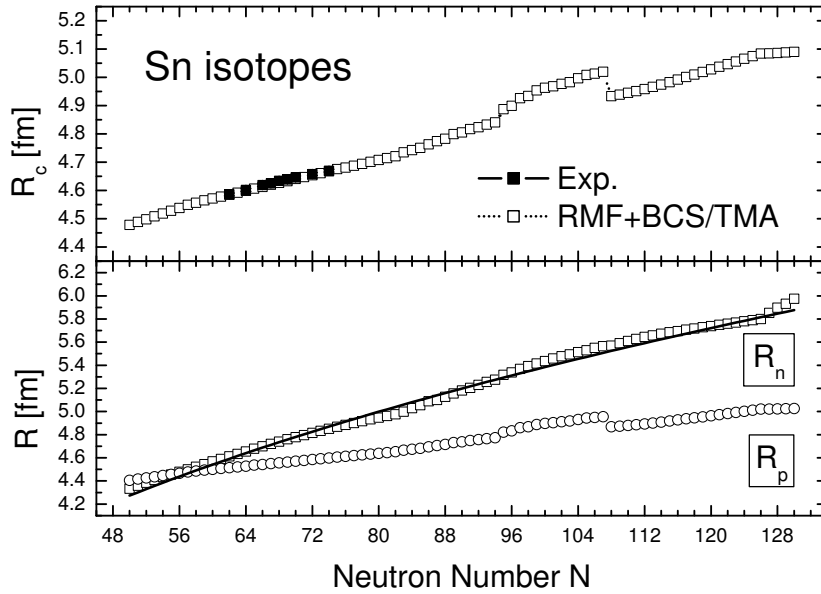


Fig. 8. Charge, proton and neutron radii obtained from the deformed RMF+BCS calculations with TMA set (open square and circle) compared with experimental data (solid square) [35]. The solid line denotes a $N^{1/3}$ dependence.

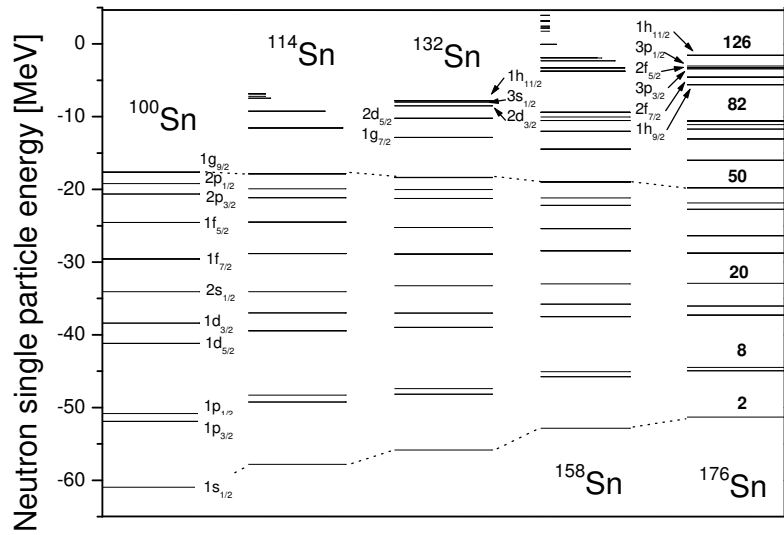


Fig. 9. Neutron single-particle spectra of ^{100}Sn , ^{114}Sn , ^{132}Sn , ^{158}Sn and ^{176}Sn obtained from the deformed RMF+BCS calculations with TMA set.